Comparison of DSMC and CFD Solutions of Fire II Including Radiative Heating

Derek S. Liechty*†, Christopher O. Johnston*
NASA Langley Research Center, Hampton, VA 23681

Mark J. Lewis‡
University of Maryland, College Park, MD 20742

The ability to compute rarefied, ionized hypersonic flows is becoming more important as missions such as Earth reentry, landing high mass payloads on Mars, and the exploration of the outer planets and their satellites are being considered. These flows may also contain significant radiative heating. To prepare for these missions, NASA is developing the capability to simulate rarefied, ionized flows and to then calculate the resulting radiative heating to the vehicle's surface. In this study, the DSMC codes DAC and DS2V are used to obtain charge-neutral ionization solutions. NASA's direct simulation Monte Carlo code DAC is currently being updated to include the ability to simulate charge-neutral ionized flows, take advantage of the recently introduced Quantum-Kinetic chemistry model, and to include electronic energy levels as an additional internal energy mode. The Fire II flight test is used in this study to assess these new capabilities. The 1634 second data point was chosen for comparisons to be made in order to include comparisons to computational fluid dynamics solutions. The Knudsen number at this point in time is such that the DSMC simulations are still tractable and the CFD computations are at the edge of what is considered valid. It is shown that there can be quite a bit of variability in the vibrational temperature inferred from DSMC solutions and that, from how radiative heating is computed, the electronic temperature is much better suited for radiative calculations. To include the radiative portion of heating, the flow-field solutions are post-processed by the non-equilibrium radiation code HARA. Acceptable agreement between CFD and DSMC flow field solutions is demonstrated and the progress of the updates to DAC, along with an appropriate radiative heating solution, are discussed. In addition, future plans to generate more high fidelity radiative heat transfer solutions are discussed.

Nomenclature

α	fraction of radiative heat flux absorbed by calorimeter
d	molecular diameter (m)
E	energy (J)
k	Boltzmann's Constant
Kn	Knudsen number
N_s	Number of species
T	Temperature (K)
V	Velocity (m/s)
X	Mole fraction
ω	Variable Hard Sphere viscosity exponent
ζ	degree of freedom

* Aerospace Engineer, Aerothermodynamics Branch, MS 408A, AIAA Member.
† Graduate Student, University of Maryland, Aerospace Engineering
‡ Professor/Department Chair, Aerospace Engineering, Room 3179 Martin Hall, AIAA Fellow, AIAA President-Elect

Subscripts

D	diameter
elec	electronic
ref	reference value
rot	rotational
s	sum over species
trans	translational
vib	vibrational
w	wall
∞	free stream

I. Introduction

In the upcoming years, the ability to compute rarefied, ionized hypersonic flows will become more and more important. Missions such as Earth reentry, landing high mass payloads on Mars, and the exploration of the outer planets and their satellites will continue to push the state of the art in direct simulation Monte Carlo (DSMC) simulations. Current major releases of most DSMC codes, including the DSMC Analysis Code (DAC) of NASA, do not include the ability to simulate ionized flows. One exception is the DSMC code DS2V, which has the ability to perform charge-neutral ionization simulations. However, this code is not parallelized, and therefore can not generally be used for large applications. To this end, DAC is currently being updated to include the ability to simulate weakly (charge-neutral) ionized flows by assuming that the electrons move along with their ions, as DS2V does. This is a very simplistic plasma simulation, but has been used in the past with some degree of success.

In addition to ionization, radiation can become an important factor depending on the mission and thermal protection system. For example, inflatable ballutes can be used to decelerate spacecraft while still high in the atmosphere. The material used for the skin of the ballute would have a very low tolerance for heating, necessitating the knowledge of what the radiative heating load would be. Several methods of calculating radiative heating for rarefied flows[1-4] have been developed. For the current study, an uncoupled methodology used in many computational fluid dynamics radiation evaluations[5, 6] was adopted as a first approximation.

Molecular-level chemistry models that predict equilibrium and non-equilibrium reaction rates using only kinetic theory and fundamental molecular properties (i.e., no macroscopic reaction-rate information) have recently been proposed[7-9] and are referred to as the Quantum-Kinetic (Q-K) chemistry model. The Q-K model has also been extended to include various reactions involving charged species[10] and to perform electronic energy level relaxation[11]. One of the upgrades currently underway for the DAC code is the inclusion of electronic energy levels as well as the aforementioned relaxation.

The primary goal of this study is to demonstrate the ability to perform DSMC simulations that include ionization and to then calculate the resultant radiative heating to the surface of a vehicle. The Fire II flight experiment was chosen for this study because of the amount of data available to compare the current solutions to. To this end, the codes DAC and DS2V are used to generate the DSMC solutions with which to compare the CFD flow field solution. The secondary goal of this paper is to report on the progress of recent upgrades to DAC, including the charge-neutral ionization model, the inclusion of electronic energy levels, and the application of the Q-K model. The appropriate temperature to be used for radiative heat transfer calculations will be discussed and the the appropriate DSMC solution will be post-processed to obtain the resultant radiative heat transfer.

The geometry of the Fire II capsule and the simulation conditions chosen for this study are first described. The two numerical methods employed in the study are next described, along with the non-equilibrium radiative heating code. Results are then presented and discussed and final conclusions are formulated.

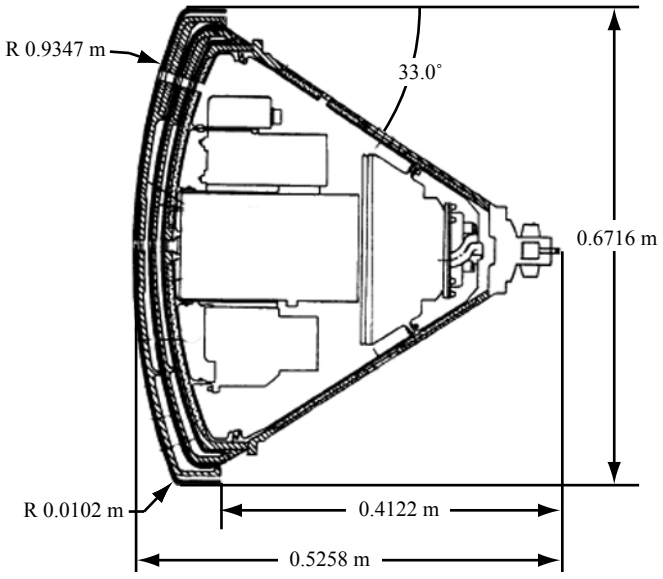

Figure 1. Geometry of the Fire II capsule.

Table 1. Free stream, surface, and geometric parameters.

Time (s)	Altitude (km)	Density (kg/m^3)	V_∞ (m/s)	T_∞ (K)	Kn_D	T_w (K)	X_{N2}	X_{O2}
1634	76.42	3.72E-05	11360	195	2.59E-03	615	0.76	0.24

Table 2. Baseline reaction rate coefficients.

Number	Reaction	k_f (m^3/molecule/s)	k_{rev} (m^3/molecule/s) (DAC)
1M	$N_2 + M \Leftrightarrow N + N + M$	$1.1624\times10^{-8}\ T^{-1.6}\ \exp(-113200/T)$	$3.0051\times10^{-44}\ T^{-0.5}$
1A	$N_2 + A \Leftrightarrow N + N + A$	$4.9982\times10^{-8}\ T^{-1.6}\ \exp(-113200/T)$	$6.3962\times10^{-40}\ T^{-1.5}$ (N only)
1E	$N_2 + e^- \Leftrightarrow N + N + e^-$	$4.9816\times10^{-6}\ T^{-1.6}\ \exp(-113200/T)$	
2M	$O_2 + M \Leftrightarrow O + O + M$	$3.3211\times10^{-9}\ T^{-1.5}\ \exp(-59360/T)$	$8.2970\times10^{-45}\ T^{-0.5}$
2A	$O_2 + A \Leftrightarrow O + O + A$	$1.6605\times10^{-8}\ T^{-1.5}\ \exp(-59360/T)$	$8.2970\times10^{-45}\ T^{-0.5}$
3 (O_2, N_2, O_2^+, N_2^+)	$NO + M1 \Leftrightarrow N + O + M1$	$8.3027\times10^{-15}\ \exp(-75500/T)$	$2.7846\times10^{-40}\ T^{-1.5}$
3 (O, N, NO, O^+, N^+, NO^+)	$NO + M2 \Leftrightarrow N + O + M2$	$3.5037\times10^{-12}\ \exp(-75500/T)$	$2.7846\times10^{-40}\ T^{-1.5}$
4	$N + e^- \Leftrightarrow N^+ + e^- + e^-$	$4.1513\times10^{4}\ T^{-3.82}\ \exp(-168200/T)$	
5	$O + e^- \Leftrightarrow O^+ + e^- + e^-$	$6.4761\times10^{3}\ T^{-3.78}\ \exp(-158500/T)$	
6	$N_2 + O \Leftrightarrow NO + N$	$9.9632\times10^{-17}\ T^{0.1}\ \exp(-38000/T)$	2.4908×10^{-17}
7	$NO + O \Leftrightarrow O_2 + N$	$1.3949\times10^{-17}\ \exp(-19400/T)$	$1.5991\times10^{-18}\ T^{0.5}\ \exp(-3600/T)$
8	$N + N \Leftrightarrow N_2^+ + e^-$	$7.3064\times10^{-23}\ T^{1.5}\ \exp(-67500/T)$	$2.4908\times10^{-8}\ T^{-1.5}$
9	$N + O \Leftrightarrow NO^+ + e^-$	$8.8009\times10^{-18}\ \exp(-31900/T)$	$2.000\times10^{-6}\ T^{-2.05}$
10	$O + O \Leftrightarrow O_2^+ + e^-$	$1.1790\times10^{-27}\ T^{2.7}\ \exp(-80600/T)$	$1.453\times10^{-4}\ T^{-2.412}$
11	$N^+ + N_2 \Leftrightarrow N_2^+ + N$	$1.6605\times10^{-18}\ T^{0.5}\ \exp(-12200/T)$	$1.295\times10^{-18}\ T^{0.5}$
12	$O^+ + N_2 \Leftrightarrow N_2^+ + O$	$1.5111\times10^{-18}\ T^{0.36}\ \exp(-22800/T)$	$4.118\times10^{-11}\ T^{-2.2}$
13	$O^+ + NO \Leftrightarrow N^+ + O_2$	$2.3248\times10^{-25}\ T^{1.9}\ \exp(-26600/T)$	$2.443\times10^{-26}\ T^{2.102}$
14	$NO^+ + N \Leftrightarrow N_2^+ + O$	$1.1956\times10^{-16}\ \exp(-35500/T)$	$1.744\times10^{-18}\ T^{0.302}$
15	$NO^+ + N \Leftrightarrow N_2 + O^+$	$5.6458\times10^{-17}\ T^{-1.08}\ \exp(-12800/T)$	$3.970\times10^{-18}\ T^{-0.710}$
16	$NO^+ + O \Leftrightarrow O_2 + N^+$	$1.6605\times10^{-18}\ T^{0.5}\ \exp(-12800/T)$	$3.040\times10^{-18}\ T^{-0.29}$
17	$NO^+ + O \Leftrightarrow O_2^+ + N$	$1.1956\times10^{-17}\ T^{0.29}\ \exp(-48600/T)$	$8.918\times10^{-13}\ T^{-0.969}$
18	$NO^+ + O_2 \Leftrightarrow O_2^+ + NO$	$3.9853\times10^{-17}\ T^{0.41}\ \exp(-32600/T)$	$3.990\times10^{-17}\ T^{0.41}$
19	$O_2^+ + N \Leftrightarrow O_2 + N^+$	$1.4447\times10^{-16}\ T^{0.14}\ \exp(-28600/T)$	
20	$O_2^+ + N_2 \Leftrightarrow N_2^+ + O_2$	$1.6439\times10^{-17}\ \exp(-40700/T)$	$4.589\times10^{-18}\ T^{-0.037}$
21	$O_2^+ + O \Leftrightarrow O^+ + O_2$	$6.6422\times10^{-18}\ T^{-0.09}\ \exp(-18000/T)$	$4.993\times10^{-18}\ T^{-0.004}$

II. Flow Conditions

The geometry of the Fire II capsule is shown schematically in Fig. 1. The forebody is spherical with a radius of 0.9347 m. In the computations, a small portion of the shoulder is included that has a radius of 0.0102 m. The computations in this study are conducted for the Fire II entry conditions at 1634 seconds, which corresponds to an altitude of 76.42 km. This point on the trajectory was chosen because the Knudsen number at this altitude based on the maximum diameter (Kn_D = 0.0026) is such that the DSMC simulations are still tractable and the CFD computations are at the boundary of what is generally considered valid. The flow conditions are provided in Table 1.

III. Numerical Methods

The two different numerical approaches applied in this study are a CFD solution of the continuum Navier-Stokes equations using the LAURA code and particle-based DSMC computations using the DS2V and DAC codes. All computations presented herein were steady state and axisymmetric with the x-direction along the axis. In each case, an 11-species (where the electron is linked to the ion for the DSMC simulations), 21-reaction, thermochemical non-equilibrium approach is adopted. The baseline 21-reaction finite rate air-chemistry model uses the rates that are listed in Table 2. The CFD solution makes use of the equilibrium constant to obtain the reverse reaction rate from the forward rate. However, the DSMC simulations do not make this assumption and therefore need the reverse rate explicitly under the Total Collision Energy (TCE) chemistry model. Because of this, the last column in Table 2 lists the reverse reaction rates used in the DSMC simulations, several of which could not be found. One difference for the DS2V chemistry set is that the charged species are not included as possible collision partners leading to dissociation of O_2, N_2, and NO. The wall temperature is assumed to be fixed at a temperature of 615 K. The wall material is assumed to be fully catalytic and ablation processes are not included in this study.

A. Details of the Continuum Flow Model

The Langley Aerothermodynamic Upwind Relaxation Algorithm (LAURA) is a high fidelity, structured grid analysis tool, specialized for hypersonic re-entry physics, utilizing state-of-the-art algorithms for computational fluid dynamic (CFD) simulations[12, 13]. Key elements of LAURA include Roe's averaging[14] and Yee's Symmetric Total Variation Diminishing (STVD)[15] formulation of second-order, inviscid flux. Yee's STVD formulation has been found to be exceptionally robust and Courant number independent using first point-implicit and then line-implicit relaxation for hypersonic flow simulations.

A two-temperature thermochemical non-equilibrium model[13] is applied and the following 11-species are included in the flowfield calculation: N, N^+, NO, NO^+, N_2, N_2^+, O, O^+, O_2, O_2^+, e^-. The chemical reaction rates are compiled from previous studies[16, 17]. The thermophysical properties are taken from the work of Mcbride, et al.[18] and Gupta, et. al.[19]. Multicomponent diffusion is approximated using Sutton and Gnoffo's[20] approximate-corrected approach.

B. Details of the Particle Flow Model

Since its introduction in the early 1960's the DSMC method of Bird[21] has become the de facto standard for simulating low-density gas dynamics. For these types of flows, traditional CFD methods are invalid because assumptions made in developing the differential equations on which they are based break down under rarefied conditions. In contrast to continuum CFD methods, the DSMC method performs a direct physical simulation of the gas at the molecular level. In the simulation, molecules are tracked in space and time, accounting for both gas-surface interactions and intermolecular collisions. The DSMC Analysis Code (DAC) software[22-24] represents NASA's state-of-the-art implementation of the DSMC method for analyzing rarefied flows. The DS2V program is a well established visual interactive DSMC program for steady or unsteady flows.

Bird[7, 9], supported by Gallis[8], have proposed a set of molecular-level chemistry models, referred to as the Quantum-Kinetic (Q-K) chemistry model, based solely on fundamental properties of the two colliding molecules: their total collision energy, their quantized vibrational energy levels, and their molecular dissociation energies. These models link chemical-reaction cross-sections to the energy-exchange process and the probability of transition between vibrational energy states. The Larsen-Borgnakke procedures[25] and the principle of microscopic reversibility are then used to derive simple, phenomenological models for the reactions. These models do not require any macroscopic data and they function by seeking to balance the fluxes into and out of each state, thus satisfying microscopic reversibility. The Q-K model has also been extended to include electronic energy level transitions[11] and also reactions involving charged species[10]. It is the electronic energy level transition model that we will be evaluating in this study.

For the current study, a simple charge-neutral ionization model was implemented where the ion and electron are linked and move together. To more closely match the continuum solution, the rotational collision number was set to 1.0 such that the molecules relax their rotational energy at every collision because the CFD solution assumes that the

Table 3. Details of DSMC cases presented.

Case	Vibrational Relaxation	Electronic Energy	Chemistry Model
DS2V	M-W (Coll. Energy)	No	TCE
DAC-I	M-W (Temp.)	No	TCE
DAC-E	M-W (Temp.)	Yes	TCE

translational and rotational temperatures are equivalent. A total of three DSMC cases are discussed and are listed in Table 3. Vibrational energy relaxation was modeled based on the data from Millikan and White[21] (M-W) with the only difference between the DS2V and DAC simulations is that DAC uses the more traditional M-W formulation[21] while DS2V uses a modified formulation[7] based on a quantized collision temperature that is anchored at two temperatures. The first temperature is the usual vibrational relaxation reference temperature for the usual reference vibrational relaxation collision number. The second temperature is the characteristic temperature of dissociation where the reference value of vibrational collision number is one. The effect of the addition of electronic energy level relaxation[11] is also examined using the DAC code. The variable hard sphere (VHS) parameters[26] used to model particle interactions are given in Table 4.

Table 4. DSMC particle parameters.

Particle	d_{ref} (m) T_{ref} = 273 K	ω
O_2	4.07E-10	0.77
N_2	4.17E-10	0.74
O	3.00E-10	0.8
N	3.00E-10	0.8
NO	4.20E-10	0.79
O_2^+	4.07E-10	0.77
N_2^+	4.17E-10	0.74
O^+	3.00E-10	0.8
N^+	3.00E-10	0.8
NO^+	4.20E-10	0.79

For this study, a charged species catalytic wall boundary condition was implemented such that any charged species, carrying along an electron, is converted to the corresponding neutral species upon impact with a wall, transferring the ionization energy to the wall.

For all of the DSMC simulations presented in this study, a grid resolved solution was unable to be obtained. For the DS2V solution, the limitation that the code is strictly serial and that the flow is dense for a DSMC simulation combine to preclude a grid resolved solution near the wall. However, the flow was resolved throughout most of the shock layer according to the rule of thumb that the mean collision separation divided by the mean free path was on the order of 0.1. The reason that a grid resolved solution was not obtained for the DAC simulation is that, as was stated earlier, the code is in the process of being updated. Recently, a code specific issue was discovered related to axisymmetric simulations at high density. This issue has recently been resolved, but there was not time to fully implement the ionization and electronic energy models such that they completely work for an adapted grid as of the writing of this paper. The implications of not having a fully resolved grid are that the reported convective heating rates will be on the order of 10% too high. The flow field properties within most of the shock layer, however, should be unaffected.

C. Details of the Non-Equilibrium Radiation Model

The shock-layer radiation is modeled with the HARA (High-temperature Aerothermodynamic RAdiation) code. The details of this code for treating air species are presented by Johnson, et al[5, 6]. Briefly, it is based on a set of atomic levels and lines obtained from the National Institute of Standards and Technology (NIST) online database[27] and the Opacity Project[28], as well as atomic bound-free cross sections from the TOPbase[29]. The negative nitrogen and oxygen ions are treated using cross sections suggested by Soon and Kunc[30] and Chauveau, et al.[31], respectively. The molecular band systems are treated using a smeared-rotational band (SRB) model[32], which was shown by Johnston, et al.[5] to be sufficient for treating VUV absorbing and optically-thin emitting band systems in air. The molecular data for modeling these band systems are obtained from Laux[33], except for the VUV N_2 systems, which are obtained from various other sources[34-36]. The non-Boltzmann modeling of the atomic and molecular electronic states is based on a set of electron-impact excitation rates compiled from the literature and presented in detail by Johnston, et al[6]. Following the work of Park[37], the quasi-steady state assumption is made when solving the Master

Equation. The tangent-slab approximation is applied to calculate radiative flux and the divergence of the radiative flux.

IV. Flow Field Results

In this section, the DSMC and CFD solutions are first compared, and then the progress of the updates to DAC are discussed, specifically the addition of electronic energy levels and their relevance to radiative heat transfer calculations. Line cuts of flow-field properties are presented in Figures 2-14. The first three Figures (2, 3, and 4) are the translational, vibrational, and electronic (CFD electronic temperature equals the vibrational temperature) temperature profiles along the axis of symmetry. The next ten Figures (5-14) are the molar fractions of O_2, N_2, O, N, NO, O_2^+, N_2^+, O^+, N^+, and NO^+, respectively.

A. Comparison of CFD and DS2V Solutions

As is shown in Fig. 2, the shock stand-off distance (location of maximum translational temperature) is in quite good agreement between the CFD and DSMC solutions. The DSMC solutions result in a slightly thicker shock (the effects of the shock are experienced further upstream) and a higher maximum translational temperature. One contributing reason for a higher translational temperature is that, even though the rotational relaxation number was set to one for the DSMC solution, there still isn't enough time for the rotational temperature (not shown) to equilibrate to the translational temperature, leaving some energy in the flow that shows up as translational temperature. However, as will be discussed later, it appears that at this free stream Knudsen number, the CFD solution breaks down in the shock front due to the increased local Knudsen number.

At first glance, the difference in vibrational temperature (Fig. 3) is quite large. However, this is partly due to a difference in the way that DS2V calculates the vibrational temperature as compared to DAC (the DAC vibrational temperatures being much closer to the CFD values). While DS2V simply takes a species weighted average over all species vibrational temperatures (including atomic species with $T_{vib} = 0$):

$$T_{vib}^{DS2V} = \sum_{s=1}^{N_s} T_{vib,s} X_s \tag{1}$$

DAC computes the vibrational temperature as an average weighted by the product of the species mole fraction and the species vibrational degrees of freedom:

$$T_{vib}^{DAC} = \frac{2E_{vib}}{k\zeta_{vib}} \tag{2}$$

where

$$E_{vib} = \sum_{s=1}^{N_s} \tfrac{1}{2} k\zeta_{vib,s} T_{vib,s} X_s \tag{3}$$

$$\zeta_{vib} = \sum_{s=1}^{N_s} \zeta_{vib,s} X_s \tag{4}$$

Another source for the discrepancy is that DS2V uses a slightly different formulation of the Millikan-White relaxation as described above. Using this new formulation of the M-W vibrational relaxation model, the collision-based temperature can result in much faster vibrational relaxation as compared to the cell temperature-based method[7], which would result in a higher vibrational temperature if the calculation was the same. Obviously, there is some ambiguity as to not only what vibrational relaxation model to use, but also on the details of how to correctly compute the vibrational temperature of a gas mixture. We will return to this point later.

When comparing the species fractions between the CFD and DSMC solutions, one must keep in mind that, first of all, there are a few reactions that aren't included in the DSMC chemistry set. Second, the reverse reaction rates are computed in very different ways. That being said, even though a direct comparison of the species concentrations isn't quite as good as hoped for, the general trends are followed. It also appears that the Knudsen effects in the

shock front are reflected in the mole fractions. For example, the trace species not found in the free stream composition are found much further upstream in the DSMC solution than for the CFD solution. This trend also appears downstream of the shock front for species such as NO, O_2^+, N_2^+, and NO^+ (Figs. 9, 10, 11, and 14). Where the CFD species fractions tend to increase rather sharply around the shock front and then decrease just as suddenly, the DSMC species fractions peak around the same level as the CFD fractions, but do so a bit downstream of them and the species can be found in greater concentrations away from the peak. For a more rigorous comparison, all possible chemical reactions should be included in each solution. One way to make sure this is possible is to make use of the Q-K chemical model since it does not require coefficients from the Arrhenius equation. More will be discussed on this later. For several of the trace species, some anomalous results seem to appear. For example, the mole fraction of O^+ for the DAC-E case seems low and the mole fraction of NO^+ for the DAC-I case seems high. Upon close examination, it was discovered that a couple of rate equations were entered in error. However, this shouldn't affect the flow field temperatures used to compute the radiative heating.

B. Effect of Electronic Energy Levels on DSMC Solution

As expected, the addition of electronic energy relaxation as an internal energy mode (DAC-I vs. DAC-E) decreased the maximum translational and vibrational temperatures. Also, even though the location of maximum translational temperature is the same between the two simulations, the region in front of the location of maximum translational temperature decreased in size when electronic energy level relaxation was added. Similar results occur when the vibrational energy mode is added to the internal modes of energy. It is simply another avenue to put kinetic energy from the free stream. Again, due to the decrease in relative translational energy available per collision, there are slightly different mole fractions between the two cases, but the trends and levels are still comparable. Using the current relaxation model, it appears that the electronic mode relaxes more quickly than the vibrational mode, resulting in a higher peak electronic temperature farther away from the body as compared to the vibrational temperature (Fig. 4).

V. Surface Heating Results

The heating values discussed herein were obtained 0.1 m from the symmetry axis and are presented in Table 5 and include the convective and radiative heating (where appropriate), as well as the sum of the convective and fraction of radiative that would have been absorbed by the calorimeter on the vehicle (α=0.72). Flight data were obtained from Cornette[38]. The DS2V, DAC-I, and CFD convective heating values compare quite well, but the DSMC solutions are not quite grid resolved near the wall due to computational resources. This generally results in convective heating values that are on the order of 10% too high. The DAC-E convective heating value is lower. This makes sense since the energy that could have been transferred to the surface is tied up in the electronic energy levels of the particles in the shock layer.

When computing the radiative heating from the DSMC solutions, one has to ask which temperature is the most appropriate to use. The CFD computation assumes that the vibrational and electronic temperatures are equal, and then this assumption is accounted for in the code HARA to estimate the actual electronic temperature from which the electronic energy levels are populated. It really doesn't make any sense to use the vibrational temperature from the DSMC simulations and make the same assumptions in HARA that are made for the CFD solution. There is no assumed electronic temperature linked to the vibrational temperature. To make matters worse, the question of which relaxation formulation and how to compute the vibrational temperature need to be answered. A much more physically appropriate strategy is to simply use the electronic temperature computed directly from the DSMC simulation (DAC-E) in order to calculate the electronic energy level distributions, bypassing any assumptions made regarding the equivalence of the vibrational and electronic temperatures. Because of the variability in definitions of the vibrational temperature and vibrational relaxation schemes, a wide range of physically impossible radiative solutions were observed that are not reported in this study. However, Table 5 does present the CFD solution, the DAC-E

Table 5. Radiation Calculation Results at z = 0.1 m.

Case	Convective Heating (W/cm^2)	Radiative Heating (W/cm^2)	$q_{conv}+\alpha q_{rad}$ (W/cm^2)
CFD	217	25	235
DS2V	220	---	---
DAC-I	220	---	---
DAC-E	195	52	232
Flight	162	18	175

solution, as well as the flight data. The DSMC radiative heating rate at the surface about twice that of the CFD and flight radiative heating rates due to a thicker shock layer and an increase in the radiator N_2^+, but the total heating seen by the calorimeter is roughly the same.

VI. Discussion

In general, the flow field comparisons between the CFD solution and the DSMC solutions are reasonable given the complex nature of the flow field and fundamental differences in simulation techniques. Trends such as a thickening of the shock layer and a higher peak translational temperature were observed, which indicate that the CFD computations are not valid in the region of the shock (the Knudsen number increases through the shock). However, it is difficult to make comparisons of the peak translational temperature and species fractions as was shown by Scalabrin[39], who compared CFD codes, and Boyd[40], who compared CFD and DSMC results. One important issue is that, for a limited number of the reverse reactions involving charged species listed in Table 2, no explicit Arrhenius equation was found for the DSMC simulations. Therefore, as was outlined in Section III, the chemistry sets between the CFD and DSMC results were slightly different. Another issue mentioned above is that, due to the increased local Knudsen number in the shock front, the shock layer is stretched out. We can see evidence of this in the translational temperature and also in the species fractions. Since the trace species are present farther up-stream of the shock front, it stands to reason that the species concentrations downstream will also be affected.

One way to address the reaction set issue would be to implement the Q-K chemistry model in the DSMC simulations. The current version of the Q-K model used in DAC is what could be called a preliminary formulation reliable for endothermic reactions (especially dissociation). The previous procedures for the corresponding exothermic reactions, however, were problematic and is why these results are not included in the current study. These issues have recently been addressed[41] and the new exothermic procedures provide a near exact match with the equilibrium constant of statistical mechanics. Unfortunately, these new procedures became available only recently and were not included in these simulations. Since the Q-K model does not depend on the availability of continuum rate coefficients, the missing exothermic reactions in Table 2 would then be able to be included in the reaction set.

The issue of this test point having a rather large Knudsen effect through the shock can only be addressed by picking another point on the trajectory, such as at 1636 seconds. At this point, the free stream Knudsen number is lower. The disadvantage of this is that the DSMC simulations will have become very computationally expensive.

The addition of electronic energy levels had an effect on the flow field properties. As discussed previously, this resulted in a decrease in the peak translational temperature and a resultant decrease in surface heating. However, the inclusion of electronic energy levels has an important implication for radiation calculations. Instead of the need to assume that the electronic temperature is equal to the vibrational temperature as HARA now does, the electronic temperature is calculated separately. This results in a more accurate representation of the electronic energy level distribution in the gas. Although the radiative heating levels are roughly twice the CFD value, the total heating to the calorimeter was the same. The largest differences between the two solutions was the electronic/vibrational temperature used and the mole fraction of N_2^+. The electronic temperature of the DAC-E simulation was higher and the peak temperature was farther away from the vehicle surface, therefore resulting in a greater distance to integrate the resulting heating to the surface. A next step in radiation calculation fidelity would be to input the potentially non-equilibrium electronic energy level distribution from the DSMC calculations directly into the radiation solver without making any assumptions of a Boltzmann distribution. This will be the focus of a follow-on study.

VII. Conclusions

Flow field comparisons have been made between DSMC and CFD solutions for the Fire II flight test at 1634 seconds. The translational temperature and most neutral species fraction comparisons between the CFD solution and the DS2V solution were reasonable with differences such as shock layer thickness and increase in translational temperature peak, including the presence of trace species upstream of the shock front. This is indicative of a breakdown in the validity of the CFD computations in the shock front due to an increase in the local Knudsen number, but comparisons such as these in the past have shown similar results. In future studies, it may be worthwhile to expend the time and resources to extend the computations down to the 1636 second conditions where the free stream Knudsen number is lower. The comparison between the CFD and DAC vibrational temperatures was good. There was, however, some discrepancy between the DAC and DS2V vibrational temperatures. One reason for the difference between the vibrational temperatures is due to how DS2V computes the vibrational temperature. Other possible sources of discrepancy are in the formulation of the vibrational relaxation scheme. Species molar fraction comparisons were not as good as hoped for, but can be partially attributed to a few reverse reactions being excluded in the DSMC solutions as well as an input error in a couple of other charged species reverse reactions, resulting in a slower rate.

In order to obtain solutions from the code DAC, updates were performed to include a weak ionization model (charge neutral) and the electronic energy transition model. The implementation of the models are not complete yet

in that an adapted solution can not yet be obtained. However, the resolution of the unadapted run was such that most of the shock layer was resolved. The results exemplify the benefits of the addition of electronic energy levels to the simulation. Also, a method to transfer DSMC solutions from a Cartesian grid to the nonequilibrium radiation solver HARA has successfully been implemented. Although the radiative heating was twice that of the CFD solution, the total heating to the surface was the same.

One way to complete the chemical reaction set and have a more natural link between the forward and reverse reaction rates for the DSMC simulations would be to implement the Quantum-Kinetic chemistry model. The current version of the Q-K model in DAC is an earlier formulation that has deficiencies when the reverse reactions are considered. An updated formulation of the Q-K model has been drafted, but has not been implemented in DAC as of the writing of this paper. It is expected that this new formulation will improve the comparisons between other DSMC simulations using the Total Collision Energy (TCE) chemistry model and also the CFD solution due to improved treatment of exothermic reactions. A major objective of the Q-K model has been to obtain a set of simple procedures that can be applied to each of the millions or billions of collisions in a DSMC application without the significant increase in the computational requirements that is associated with the existing TCE model. The Q-K rates are now in near exact agreement with the equilibrium constant of statistical mechanics, but the constant does not have to be calculated within the DSMC implementation. A further advantage of the Q-K procedures over the TCE procedures is that their derivation does not employ equilibrium kinetic theory and can be applied with greater confidence to very fast reactions that may involve large distortions of the equilibrium velocity distribution. While these are important considerations, the major advantage of the Q-K model is that it does not depend on the availability of rate coefficients that are based primarily on experiment. Further work is required in implementing the new formulation of the Q-K model into current software.

Comparisons were also made between DSMC simulations with and without electronic energy levels. The results were as expected: the peak translational temperature in the shock layer decreased and the surface heating decreased. Current best practices for nonequilibrium radiation solvers are to assume that the electronic temperature is linked with the vibrational temperature in the CFD code and then make corrections to this temperature to obtain the electronic temperature in the radiation code. The addition of electronic energy levels to the DSMC computations negates the necessity of this assumption, but results in higher radiative heating levels. The current radiative heating comparison between DSMC and CFD is not satisfactory, but the total heating to the surface is the same as the CFD value. These are, as stated before, preliminary results and there are several important issues to address before any statements as to which answer is correct can be made. This has been a continuing step to test the new electronic energy relaxation algorithm. Since this algorithm was based on the original Q-K model, it is possible that a reformulation may be necessary for the exothermic transitions. The next logical step for radiation calculations would be to input the nonequilibrium distribution of electronic energy levels from the DSMC simulation directly into the radiation solver.

There are several items that must be addressed in order to make a better one-to-one comparison between DSMC and CFD computations of ionized flows including radiation. First, the precise reason that the DS2V vibrational temperature is so different from the CFD and DAC vibrational temperatures must be identified. Second, the Q-K model, in it's newest formulation, must be incorporated into the DAC code so that the chemical reaction sets, both forward and reverse, are similar between the CFD and DSMC computations and that the principle of detailed balance be satisfied.

VII. Acknowledgements

The authors would like to acknowledge the support of the Exploration Technology Development and Demonstration (ETDD) Program, managed at NASA-Glenn Research Center. The work documented herein was performed as part of ETDD's Entry, Descent, and Landing (EDL) Technology Development Project, which is managed at NASA-Langley Research Center and supported by NASA-Ames Research Center, NASA-Johnson Space Center, and the Jet Propulsion Laboratory.

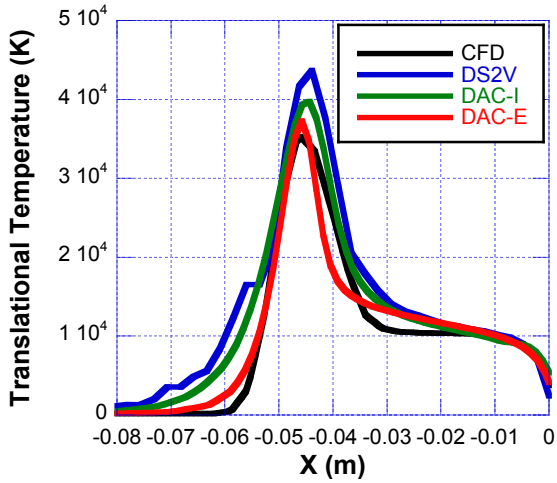

Figure 2. Translational temperature comparison.

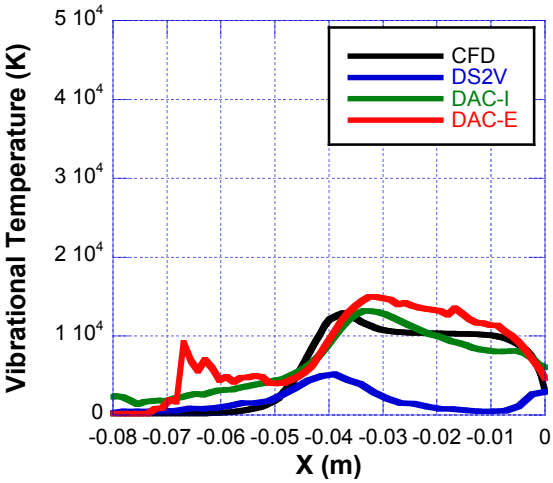

Figure 3. Vibrational temperature comparison.

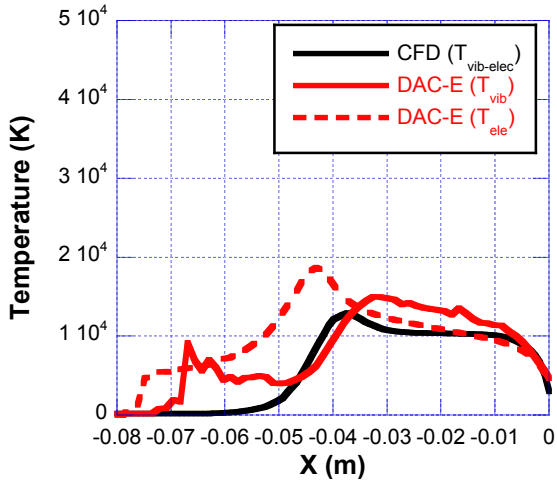

Figure 4. Electronic temperature.

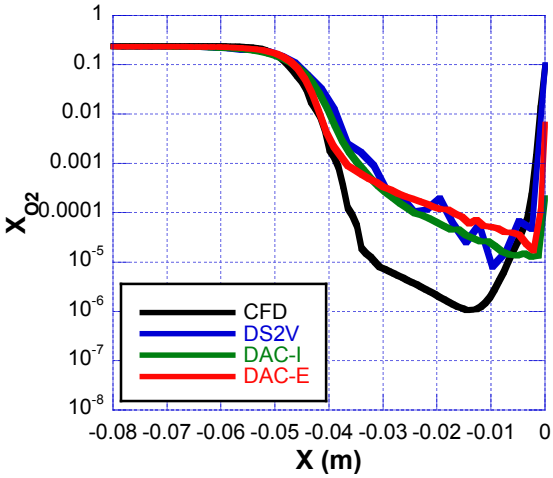

Figure 5. O_2 mole fraction comparison.

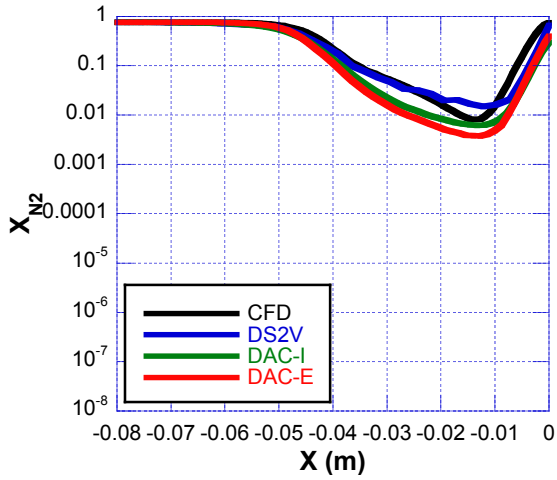

Figure 6. N_2 mole fraction comparison.

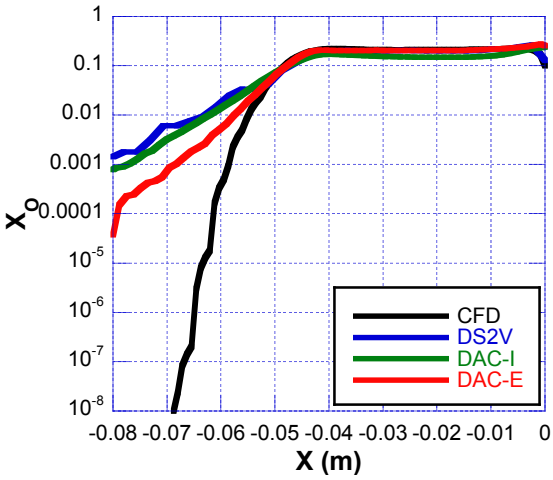

Figure 7. O mole fraction comparison.

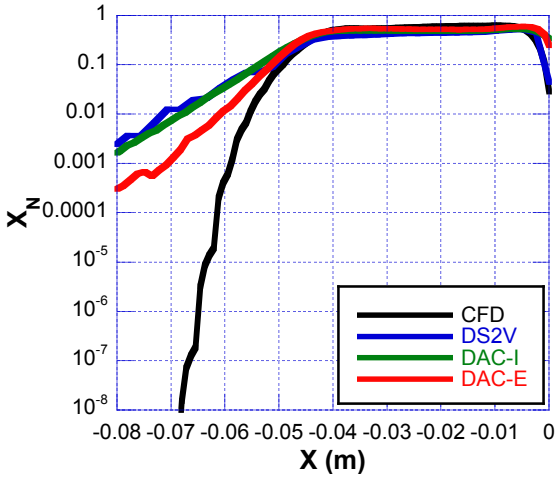

Figure 8. N mole fraction comparison.

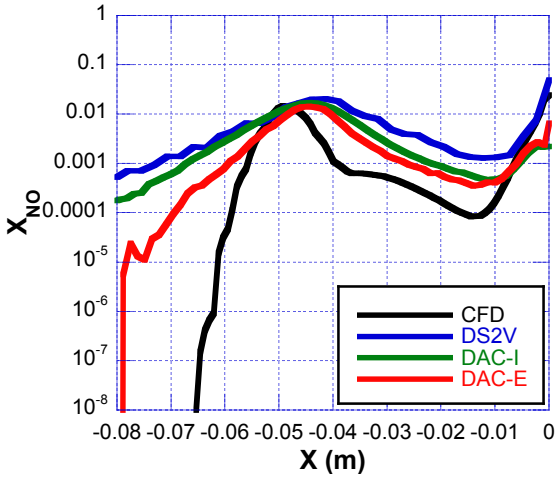

Figure 9. NO mole fraction comparison.

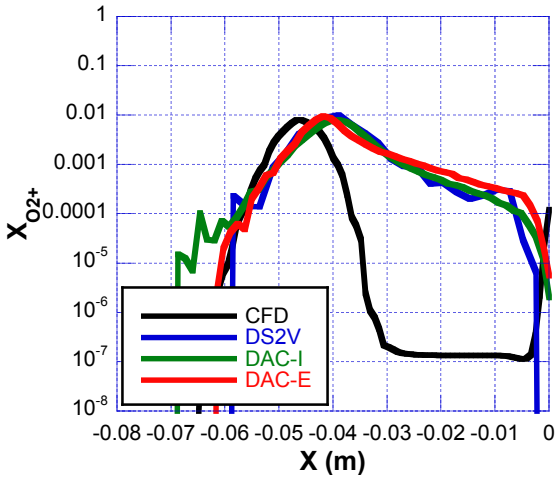

Figure 10. O_2^+ mole fraction comparison.

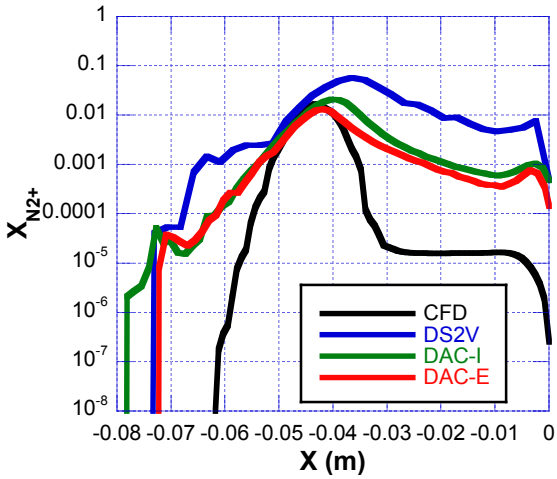

Figure 11. N_2^+ mole fraction comparison.

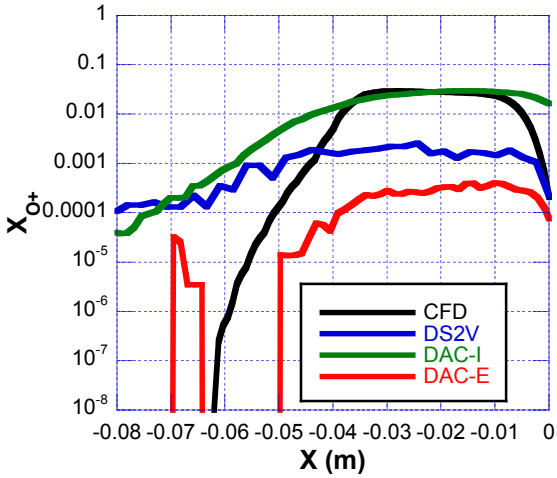

Figure 12. O^+ mole fraction comparison.

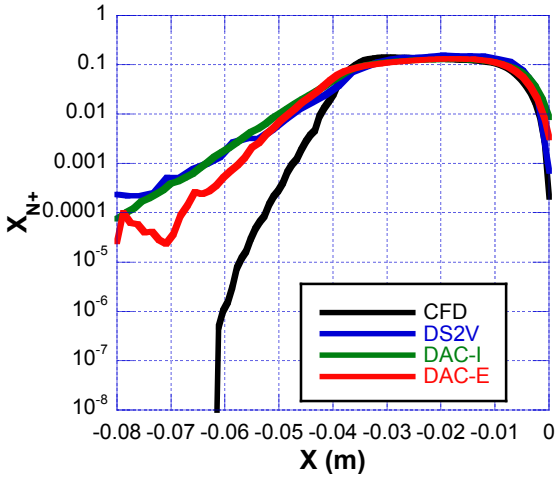

Figure 13. N^+ mole fraction comparison.

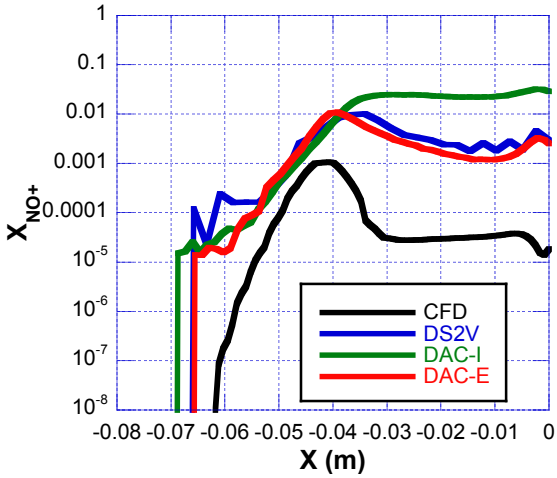

Figure 14. NO^+ mole fraction comparison.

References

[1] Bird, G. A. "Nonequilibrium Radiation During Re-Entry at 10 km/s." AIAA 1987-1543, 1987.

[2] Gallis, M. A., and Harvey, J. K. "Nonequilibrium Thermal Radiation from Air Shock Layers Modeled with Direct Simulation Monte Carlo," *Journal of Thermophysics and Heat Transfer* Vol. 8, No. 4, 1994, pp. 765-772.

[3] Carlson, A. B., and Hassan, H. A. "Radiation Modeling with Direct Simulation Monte Carlo," *Journal of Thermophysics and Heat Transfer* Vol. 6, 1992, pp. 631-636. doi: 10.2514/3.11544

[4] Ozawa, T., Levin, D. A., Wang, A., and Modest, M. "Development of Coupled Particle Hypersonic Flowfield-Photon Monte Carlo Radiation Methods," *Journal of Thermophysics and Heat Transfer* Vol. 24, No. 3, 2010, pp. 612-622.

[5] Johnston, C. O., Hollis, B. R., and Sutton, K. "Spectrum Modeling for Air Shock Layers at Lunar Return Conditions," *Journal of Spacecraft and Rockets*, Accepted for publication.

[6] Johnston, C. O., Hollis, B. R., and Sutton, K. "Non-Boltzmann Modeling for Air Shock Layers at Lunar Return Conditions," *Journal of Spacecraft and Rockets*, Accepted for publication.

[7] Bird, G. A. "A Comparison of Collision Energy-based and Temperature-based Procedures in DSMC," *Rarefied Gas Dynamics, 26th Symposium*. Vol. 1084, American Institue of Physics, Kyoto, Japan, 2009, pp. 245-250.

[8] Gallis, M. A., Bond, R. B., and Torczynski, J. R. "A kinetic-theory approach for computing chemical-reaction rates in upper-atmosphere hypersonic flows," *The Journal of Chemical Physics* Vol. 131, No. 12, 2009, p. 124311. doi: 10.1063/1.3241133

[9] Bird, G. A. "Chemical Reactions in DSMC," *Rarefied Gas Dynamics, 27th Symposium*. American Institute of Physics, Pacific Grove, CA, 2010.

[10] Liechty, D. S., and Lewis, M. J. "Extension of a Kinetic-Theory Approach for Computing Chemical-Reaction Rates to Reactions with Charged Particles," *27th International Symposium on Rarefied Gas Dynamics*. AIP, Asilomar, CA, 2010.

[11] Liechty, D. S., and Lewis, M. J. "Treatment of Electronic Energy Level Transition and Ionization Following the Particle-Based Chemistry Model." AIAA 2010-449, 2010.

[12] Cheatwood, F. M., and Gnoffo, P. "User's Manual for the Langley Aerothermodynamic Upwind Relaxation Algorithm (LAURA)." NASA TM 4674, April 1996.

[13] Gnoffo, P., Gupta, R. N., and Shinn, J. L. "Conservation Equations and Physical Models for Hypersonic Air Flows in Thermal and Chemical Nonequilibrium," *NASA TP 2867*. Feb. 1989.

[14] Roe, P. L. "Approximate Riemann Solvers, Parameter Vectors, and Difference Schemes," *Journal of Computational Physics* Vol. 43, No. 2, 1981, pp. 357-372.

[15] Yee, H. C. "On Symmetric and Upwind TVD Schemes," *NASA TM 88325*. 1986.
[16] Park, C. "Review of Chemical-Kinetic Problems of Future NASA Missions, I: Earth Entries," *Journal of Thermophysics and Heat Transfer* Vol. 7, 1993, pp. 385-398.

[17] Park, C., Jaffe, R. L., and Partridge, H. "Chemical-Kinetic Parameters of Hyperbolic Earth Entry," *Journal of Thermophysics and Heat Transfer* Vol. 15, No. 1, 2001, pp. 76-90.

[18] Mcbride, B. J., Zehe, M. J., and Gordon, S. "NASA Glenn Coefficients for Calculating Thermodynamic Properties of Individual Species." NASA TP 2002-211556, Sept. 2002.
[19] Gupta, R. N., Yos, J. M., Thompson, R. A., and Lee, K. P. "A Review of Reaction Rates and Thermodynamic and Transport Properties for an 11-Species Air Model for Chemical and Thermal Nonequilibrium Calculations to 30,000 K." NASA RP-1232, 1990.
[20] Sutton, K., and Gnoffo, P. "Multi-Component Diffusion with Application to Computational Aerothermodynamics." AIAA Paper 98-2575, 1998.
[21] Bird, G. A. *Molecular Dynamics and the Direct Simulation of Gas Flows*. Oxford, UK: Oxford University Press, 1994.
[22] Wilmoth, R. G., LeBeau, G. J., and Carlson, A. B. "DSMC Grid Methodologies for Computing Low-Density, Hypersonic Flows About Reusable Launch Vehicles." AIAA 1996-1812, 1996.
[23] LeBeau, G. J. "A Parallel Implementation of the Direct Simulation Monte Carlo Method," *Computer Methods in Applied Mechanics and Engineering* Vol. 174, No. 3-4, 1999, pp. 319-337.

[24] LeBeau, G. J., Boyles, K. A., and Lumpkin III, F. E. "Virtual Sub-Cells for the Direct Simulation Monte Carlo Method." AIAA 2003-1031, 2003.
[25] Borgnakke, C., and Larsen, P. S. "Statistical collision model for Monte Carlo simulation of polyatomic gas mixtures," *Journal of Computational Physics* Vol. 18, 1975.
doi: 10.1016/0021-9991(75)90094-7
[26] Bird, G. A. "Monte Carlo Simulation in an Engineering Context," *AIAA Progress in Astronautics and Aeronautics: Rarefied Gas Dynamics*. Vol. 74, Part I, AIAA, New York, 1981, pp. 239-255.
[27] Ralchenko, Y., and al., e. "NIST Atomic Spectra Database, Version 3.1.0." National Institute of Standard and Technology (NIST) Physics Lab, http://physics.nist.gov/PhysRefData/ASD/index.html, July 2006.
[28] Team, T. O. P. *The Opacity Project, Vol. 1*. Bristol and Philedelphia: Institute of Physics Publishing, 1995.
[29] Cunto, W., and al, e. "TOPbase at the CDS," *Astronomy and Astrophysics* Vol. 275, 1993, pp. L5-L8.

[30] Soon, W. H., and Kunc, J. A. "Nitrogen Plasma Continuum Emission Associated with N-(3P) and N-(1D) Ions," *Physical Review A* Vol. 41, 1990, pp. 4531-4533.

[31] Chauveau, S., Deron, C., Perrin, M. Y., Riviere, P., and Soufiani, A. "Radiative Transfer in LTE Air Plasmas for Temperatures up to 15,000 K," *Journal of Qualitative Spectroscopy and Radiative Transfer* Vol. 77, 2003, pp. 113-130.

[32] Chambers, L. H. "Predicting Radiative Heat Transfer in Thermochemical Nonequilibrium Flow Fields." NASA TM-4564, 1994.
[33] Laux, C. O. "Optical Diagnostics and Radiative Emission of Air Plasmas." High Temperature Gas Dynamics Lab, Mechanical Engineering Dept., Rept. T-288, Stanford University, 1993.
[34] Whang, T. J., Guoxing, Z., Stwalley, W. C., and Wu, C. Y. R. "Franck-Condon Factors of the ..... Transitions of N2," *Journal of Quantitative Spectroscopy and Radiative Transfer* Vol. 55, 1996, pp. 335-344.

[35] Stahel, D., Leoni, M., and Dresslar, K. "Nonadiabatic Representations of the 1Σu and 1Πu States of the N2 Molecule," *Journal of Chemical Physics* Vol. 79, Sept. 1983, pp. 2541-2558.

[36] Chauveau, S., Perrin, M. Y., Riviere, P., and Soufiani, A. "Contributions of Diatomic Molecular Electronic Systems to Heated Air Radiation," *Journal of Quantitative Spectroscopy and Radiative Transfer* Vol. 72, 2002, pp. 503-530.

[37] Park, C. "Radiation Enhancement by Nonequilibrium in Earth's Atmosphere," *Journal of Spacecraft and Rockets* Vol. 22, 1985, pp. 27-36.

[38] Cornette, E. S. "Forebody Temperature and Calorimeter Heating Rates Measured During Project Fire II Reentry at 11.35 km/s." NASA TM X-1305, 1966.
[39] Scalabrin, L. C., and Boyd, I. D. "Numerical Simulations of the FIRE-II Convective and Radiative Heating Rates." AIAA 2007-4044, 2007.
[40] Boyd, I. D., Trumble, K., and Wright, M. "Nonequilibrium Particle and Continuum Analyses of Stardust Entry for Near-Continuum Conditions." AIAA 2007-4543, 2007.
[41] Bird, G. A. "The Q-K Model for Gas-Phase Chemical Reaction Rates," *To Appear in Physics of Fluids*, 2011.